International Journal of Nanomedicine

Dovepress
open access to scientific and medical research

Open Access Full Text Article

ORIGINAL RESEARCH

Breakthrough of Hypoxia Limitation by Tumor-Targeting Photothermal Therapy-Enhanced Radiation Therapy

Yi Zhang[1], Dang Liu[2], Bin Qiao[3], Yuanli Luo[3], Liang Zhang[3], Yang Cao[3], Haitao Ran[3,*], Chao Yang[4,*]

[1]Department of Ultrasound, the First Affiliated Hospital of Chongqing Medical University, Chongqing, People's Republic of China; [2]Department of Radiology, the Second Affiliated Hospital of Chongqing Medical University, Chongqing, People's Republic of China; [3]Chongqing Key Laboratory of Ultrasound Molecular Imaging & Department of Ultrasound, the Second Affiliated Hospital of Chongqing Medical University, Chongqing, People's Republic of China; [4]Department of Radiology, Jiulongpo District People's Hospital, Chongqing, People's Republic of China

*These authors contributed equally to this work

Correspondence: Haitao Ran, Chongqing Key Laboratory of Ultrasound Molecular Imaging & Department of Ultrasound, the Second Affiliated Hospital of Chongqing Medical University, Chongqing, People's Republic of China, Tel +86 13512373563, Email ranhaitao@cqmu.edu.cn; Chao Yang, Department of Radiology, Jiulongpo District People's Hospital, Chongqing, People's Republic of China, Tel +86 13883095836, Email ychaof737@163.com

Purpose: To address the problem of suboptimal reactive oxygen species (ROS) production in Radiation therapy (RT) which was resulted from exacerbated tumor hypoxia and the heterogeneous distribution of radiation sensitizers.

Materials and Methods: In this work, a novel nanomedicine, designated as PLGA@IR780-Bi-DTPA (PIBD), was engineered by loading the radiation sensitizer Bi-DTPA and the photothermal agent IR780 onto poly(lactic-co-glycolic acid) (PLGA). This design leverages the tumor-targeting ability of IR780 to ensure selective accumulation of the nanoparticles in tumor cells, particularly within the mitochondria. The effect of the photothermal therapy-enhanced radiation therapy was also examined to assess the alleviation of hypoxia and the enhancement of radiation sensitivity.

Results: The PIBD nanoparticles exhibited strong capacity in mitochondrial targeting and selective tumor accumulation. Upon activation by 808 nm laser irradiation, the nanoparticles effectively alleviated local hypoxia by photothermal effect enhanced blood supplying to improve oxygen content, thereby enhancing the ROS production for effective RT. Comparative studies revealed that PIBD-induced RT significantly outperformed conventional RT in treating hypoxic tumors.

Conclusion: This design of tumor-targeting photothermal therapy-enhanced radiation therapy nanomedicine would advance the development of targeted drug delivery system for effective RT regardless of hypoxic microenvironment.

Keywords: Bi-DTPA, IR780, radiotherapy, tumor microenvironment hypoxia, photothermal therapy

Introduction

RT (radiotherapy) is an effective measure which is commonly used to treat cancers in clinic, and residual lesions in advanced cancers that failed to be removed by surgery can be obliterated by RT, by which patients can achieve longer survival time.[1,2] The high energy ionizing radiation in X ray kills cancer cells by cytotoxic oxygen radical (Reactive oxygen species, ROS) produced during ionization, of which the process is not limited by lesion depth.[3] Nevertheless, the therapeutic effect of RT is constrained because of tumor-microenvironment (TME)-related irradiation resistance and peripheral normal tissue damages caused by high energy ionizing radiation,[4] which could result in incomplete elimination of tumor cells, tumor recurrence and metastasis.[5,6] Although increasing X ray dosage can effectively kill tumor cells, it causes severe damages to normal tissues irreversibly and inevitably, resulting in serious adverse effects.

High Z number metallic ion Bi, can effectively absorb, scatter and re-emit radiation to augment radiation dosage in local lesion, which can be recognized as a sound radiation sensitizer that reduces X ray dosage and adverse effects.[7,8]

Received: 29 December 2023
Accepted: 11 June 2024
Published: 26 June 2024

However, TME hypoxia, a common characteristic of solid tumors, strongly restricts the oxygen-dependent production of ROS.[9] Moreover. Local hypoxia is aggravated by the continual consumption of oxygen during RT, leading to severe reduction of of ROS.[10] Researchers have been exploiting various methods to relieve hypoxia in tumors, such as delivering exogenous oxygen, and increasing endogenous oxygen in tumors by biocatalysis.[11] However, due to the complexity in vivo physiological environment, improvements in nonspecific distribution and inefficient catalysis are still in demand to avoid potential systematic biosafety issues and unsatisfactory relief of hypoxia.[12]

Previous studies have proposed that the intracellular localization of nanodrugs has crucial influence on therapeutic effects.[13] In details, as an essential organelle that provides energy for cells, as well as a key regulatory factor of apoptosis, mitochondria possesses the potential to work as an ideal target for treatment.[14,15]

Thermal effect can accelerate blood circulation in tumor area, and consequently improve TME hypoxia.[16,17] Thermal-effect-based Photothermal Therapy (PTT) is characterized by non-invasion and non-drug-resistance,[18,19] and can efficiently enhance the anti-cancer effect of tumor mitochondria-targeting RT by increasing oxygen-dependent ROS production. Therefore, we proposed a new strategy based on enhancing tumor mitochondria-targeting RT by PTT conquering TME hypoxia. Specifically, the promoted production of ROS could be due to PTT increased blood supply in tumor area and improved the utilization of oxygen, which eventually realized cascade amplification of RT effect.

Herein, we report a tumor mitochondria-targeted nanodrug which realizes cascade amplification of RT by photothermal effect. With the non-radioactive high Z number element Bi, Bi-DTPA possesses stronger RT sensitization ability than iodine Which is commonly applied in clinic. Meanwhile, the application of Bi in CT imaging has been proved to be valuable, by which the biological distribution of the nanodrug could be potently monitored.[20–23] A hydrophilic Bi-based RT sensitizer namely Bi-DTPA was synthesized by the one-pot method which has advantages such as low-cost, feasibility in quantity production and good biocompatibility.[24,25] IR780, commonly known as a tumor-mitochondria-specific photosensitizer, exhibits good photothermal effect which can produce thermal energy under proper laser irradiation,[26] and consequently increase local oxygen supply in the tumor area, conquer hypoxia in tumor tissues and enhance the therapeutic effect of RT.[16,17,27] Moreover, its properties in optical imaging and photoacoustic (PA) imaging endow nanodrug with iconography-information-collecting function.[26,28] The nanodrug named PIBD was constructed by the combined loading of Bi-DTPA and IR780 on PLGA-a biosafe material approved by the Food and Drug Administration (FDA). PIBD nanoparticles were intravenously injected into tumor-bearing mice models, after which nanoparticles efficiently accumulated in tumor area with the guidance of IR780, produced thermal energy to increase local blood supply under proper laser irradiation, and improved therapeutic effect of RT by conquering TME hypoxia, eventually cascade amplification of RT effect was realized (Scheme 1).

Materials and Methods

Bi_2O_3, DTPA and NaOH were purchased from RON's reagent company; 1640 cell culture medium, Penicillin-streptomycin antibiotic, phosphate buffered saline (PBS), Giemsa dye, Triton X-100, Dimethyl sulfoxide (DMSO), methanol, DCFH-DA, dichloromethane, DAPI, tween-20, DiI, Mito-Tracker green and isopropanol were purchased from Beyotime Biotechnology; Iopromide 370 was purchased from Bayer Schering Pharma AG; CCK-8 kit was purchased from Dojindo Laboratories; fetal bovine serum and bovine albumin (BSA) were purchased from Gibco; Anti-phospho-histone γ-H2AX Mouse monoclonal antibody and Goat Anti-Mouse IgG H&L were purchased from Abcam. 4T1 cells (Mouse breast cancer cells) was purchased from Wuhan Punosai Life Technology Co., LTD.

Synthesis and Characterization of PIBD

Bi-DTPA was synthesized by one-pot method. In details. Firstly, Bi_2O_3 (0.5mmol) and DTPA (1mmol) were mixed and dissolved in 20mL of double distilled water and heated at 85°C for 2 hours, followed by lyophilization after pH was adjusted to 7 by NaOH.

PIBD nanoparticle was synthesized by double emulsification method. In details, 2 mg of IR780 and 50 mg of PLGA were dissolved in 2 mL of dichloromethane as the organic phase, then 200 μL of Bi-DTPA solution (1g/mL) was added as the aqueous phase. The mixture was then treated by Ultrasonic Processor (Sonics&Materials) for 3 minutes under ice bath (parameters were set as 54 W, time interval of 5 seconds). Then 10 mL of PVA solution (5%) was added, and the ultrasonic

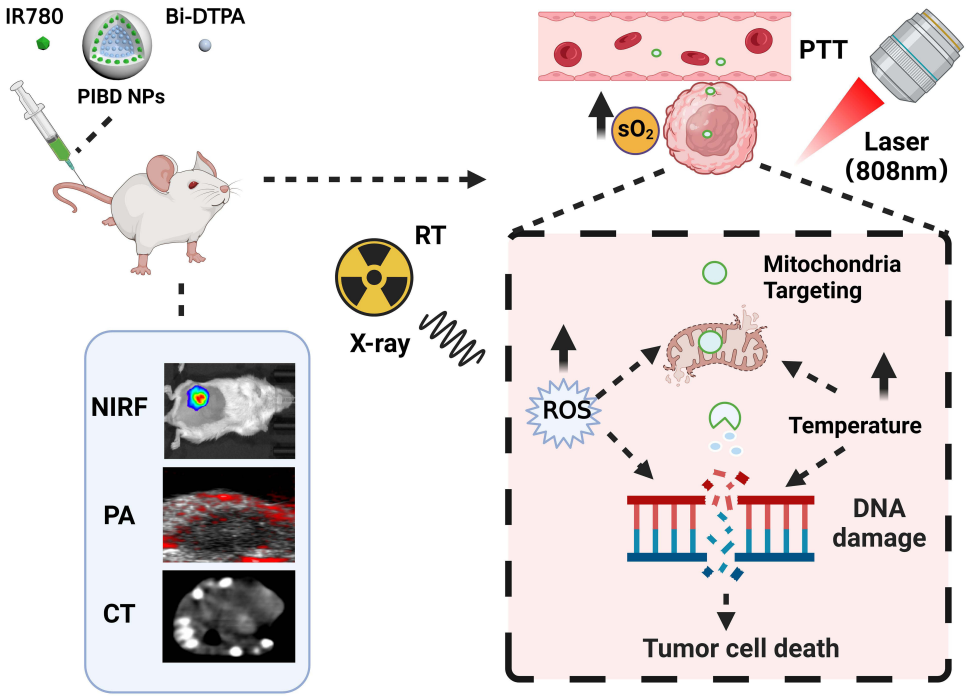

Scheme 1 Preparation of PIBD and mechanism of action of multi-mode imaging, phototherapy combined with radiotherapy.

vibration process applied above was conducted again under the same conditions followed by adding 10 mL of isopropanol solution (2%), and the final mixture was magnetically stirred for one hour and stilled for two hours to evaporate dichloromethane in a biosafety cabinet. Eventually, the evaporated mixture was centrifuged (4725 x g, 5 min) and washed by double distilled water for 3 times. The final precipitation was re-suspended with 2 mL of double distilled water and stored at 4°C.

The size and zeta potential of PIBD were detected by Malvern nanosizer (Brookhaven Omni); the surface morphology and elements distribution were observed by SEM-EDS (Jeol); the internal structure was analyzed by TEM (Hitachi); The UV absorption peak was measured by UV spectrophotometer (Shimadzu). A small amount of PIBD was added to mouse serum, refrigerated for 1 week, and the size changes were detected by Marvin particle size analyzer on the 1st, 3rd, 5th and 7th day, respectively.

IR780 was dissolved by DMSO and diluted into different concentrations (0, 0.78, 1.56, 3.12, 6.25, 12.5 μg/mL). To plot the OD/concentration standard curve of IR780, UV spectrophotometer (Shimadzu) was used to detect the corresponding OD values of the solutions at the wavelength ranged from 500nm to 900nm. The supernatant collected during synthesis was detected by an UV spectrophotometer, and the concentration of IR780 was calculated according to the standard curve. Then the encapsulation rate and loading capacity were calculated according to following equations:

Encapsulation rate (%) = (IR780 input- IR780 in supernatant)/IR780 input*100%

Loading capacity (%) = (IR780 input- IR780 in supernatant)/PLGA input*100%

Bi-DTPA was dissolved by double distilled water and diluted into different concentrations (0, 0.078, 0.156, 0.312, 0.625, 1.25mg/mL). To plot the OD/concentration standard curve of Bi-DTPA, UV spectrophotometer (Shimadzu) was used to detect the corresponding OD values of the solutions at the wavelength ranged from 270nm to 350nm. The supernatant collected during synthesis was detected by an UV spectrophotometer, and the concentration of Bi-DTPA was calculated according to the standard curve. Then the encapsulation rate and loading capacity were calculated according to following equations:

Encapsulation rate (%) = (Bi-DTPA input- Bi-DTPA in supernatant)/Bi-DTPA input*100%

Loading capacity (%) = (Bi-DTPA input- Bi-DTPA in supernatant)/PLGA input*100%

Biosafety of PIBD

In vitro Biosafety

4T-1 cells were seeded in 96-well plate at a density of 5×10^3 per well, and treated with PIBD (100 μL/well) at different concentrations (0, 1, 1.5, 2, 2.5, 3mg/mL) for 24 h, after which the supernatant was discard and cells were washed for 3 times by PBS. Cell viability was detected by CCK8-kit (Optical density; OD value) (Bio-Rad). Cell viability was calculated according to following formula.

Cell viability (%) = (OD value of experimental group – OD value of blank group)/(OD value of control group – OD value of blank group) × 100%

In vivo Biosafety

A total of 125 Balb/c mice were randomly divided into 5 groups, including a control group treated with saline and 4 experimental groups treated with 200 μL of PIBD (5mg/mL) through caudal vein. Mice were orderly euthanized on the day before injection (pre), day 3, 7, 14, 30. The blood and serum were collected for blood routine examination (HGB, HCT, MCHC, PLT, MCV, MCH, WBC, RBC) and serum biochemical index examination (ALT, AST, BUN, CRE). H&E staining was performed to estimate whether main organs were affected, including heart, liver, spleen, lung and kidney.

Detection of Drug Metabolism in vivo

A total of 40 Balb/c mice were randomly divided into 8 groups and treated with PIBD 200 μL (5mg/mL) through caudal vein. Mice were orderly euthanized on the 0.5h, 1h, 6h, 12h, 24h, 30h, 48h, and 72h. Blood was collected and sent to ICP to detect Bi element content in blood.

Tumor Mitochondria-Targeting Ability of PIBD

DiI (1 mg) was additionally added in the organic phase during the synthetic process to prepare DiI-tagged PIBD and PBD. These nanoparticles were co-incubated with 4T1 cells for 12 hours. Then cells were washed by PBS for 3 times to remove residual nanoparticles, and Mito-Tracker green was used to mark cell mitochondria. After 30-minute incubation, cells were washed by PBS for three times, and DAPI (100μL) was used to mark cell nucleus. Cells were again washed by PBS for 3 time to remove residual DAPI, and observed under CLSM to estimate the co-localization between nanoparticles and mitochondria. The Image J software was used for Colocalization analysis and quantitative analysis. Colocalization quantitative analysis results were Pearson's correlation coefficient, −1 ~ 0.5 indicates no co-location. 0.5 ~ 1 indicates co-location.

In vitro Photothermal Effect of PIBD

PIBD at different concentrations (0,1.25,2.5,5,10 mg/mL) were considered as the variable and placed in 96-well plate (200 μL/well). Laser 808nm (Mid-River) were applied to wells at a power of $1 W/cm^2$, and the change of temperature was recorded. Additionally, laser 808nm at different powers (0, 0.5, 1, 1.5, 2, 2.5 W/cm^2) were set as the variable, the variation of the temperature of PIBD (5mg/mL) was recorded. The photothermal effect induced by PIBD was evaluated according to the recorded temperature variation.

Multi-Modality Imaging by PIBD

Establishment of 4T1 Tumor Bearing Mouse Model of Breast Cancer

4T1 cells were cultured with 1640 cell culture medium containing 10% of fetal bovine serum and 1% of penicillin-streptomycin solution in an incubator with 5% CO_2 at 37°C (the latter culture conditions were the same), and resuspended in Phosphate buffered saline (PBS) after digestion by trypsin, after the mice skin was disinfected with 75% alcohol, 100 μL of 4T1 cells (1×10^6 cells) in logarithmic growth phase were injected subcutaneously on the back of nude mice. Treatments were performed when the tumor grew to a volume of 75 mm^3 after 2–3 weeks.

CT Imaging in vitro/ Vivo

PIBD nanoparticle was diluted into a set of concentrations, including 0, 1.5625, 3.125, 6.25, 12.5, 25 mg/mL, and kept in EP tubes for CT scanning, and CT values were recorded. Tumor-bearing mice were anesthetized by 1% of pentobarbitone, and the Pre PA image was collected before mice were intravenously injected with 200 μL of PIBD nanoparticles (5mg/mL). CT scanning was performed on tumor-bearing mice, and CT images were captured at the time points of 1h, 6h, 12h, 24h, 30h, and the corresponding CT values were recorded and analyzed.

Photoacoustic Imaging in vitro/ Vivo

Cuboid agarose gel model was prepared by melting and solidifying 500 mL of agarose solution (3%). Nanoparticles were diluted into different concentrations (0, 2.5, 5, 7.5, 10, 12.5mg/mL), and 200 μL of nanoparticles at each concentration was added in the gel model. In vitro PA imaging was performed on the gel model at a wavelength of 780nm by photoacoustic imager (Visual Sonics), and PA values were recorded and analyzed. Tumor-bearing mice were anesthetized by 1% of pentobarbitone, and the Pre PA image was captured before intravenously injection of 200μL of PIBD nanoparticles (5mg/mL). Photoacoustic imaging was performed on tumor areas at a wavelength of 780nm, and images were captured at the time points of 1h, 6h, 12h, 24h, 30h, and the corresponding PA values were recorded and analyzed.

NIFR Imaging in vitro/ In vivo

PIBD nanoparticle was diluted to a set of concentrations, including 0, 1.5625, 3.125, 6.25, 12.5, 25 mg/mL. 100 μL of nanoparticles at each concentration was added into 96-well black opaque plate, and irradiated by an optimal laser (excitation/emission=745nm/820nm) (PerkinElmer) to obtain NIRF images, the corresponding fluorescence values were recorded and analyzed. Tumor-bearing mice were anesthetized by 1% of pentobarbitone, and the Pre NIRF image was collected before mice were intravenously injected with 200 μL of PIBD nanoparticles (5mg/mL). NIRF imaging was captured at the wavelength of 745/820nm at the time points of 1h, 6h, 12h, 24h, 30h, and the corresponding fluorescence values were recorded and analyzed. Twenty-four hours after the injection, mice were euthanized. Tissues including heart, liver, spleen, lung, kidney and tumor were collected and irradiated with laser (745nm/820nm) to obtain NIRF images, and the corresponding fluorescence values were recorded and analyzed.

PTT-RT Combined Therapy

In Vitro

4T1 cells were divided into the following groups: ①Control; ②NIR; ③X-ray; ④X-ray+NIR; ⑤PIBD+NIR; ⑥PIBD +X-ray; ⑦PIBD+X-ray+NIR。X-ray was applied at a dosage of 6Gy; the applied wavelength of NIR was 808nm, power was set at 1W/cm^2. The procedures of other in vivo therapies were consistent with those of the imaging process.

CCK8 Assay

4T1 cells were seeded in 96-well plate at a concentration of 5*10^3 per well and divided into 7 groups, and each group included 5 replicates. After the corresponding treatments were applied, cells were added with CCK8 agent and detected by microplate reader to gain OD value at a wavelength of 450 nm to assess cell viability.

The Detection of Reactive Oxygen Species (ROS)

4T1 cells were seeded in confocal dishes at the concentration of 3*10^4 cells/dish and incubated overnight for attachment. Then, 1 mL of 2',7'-Dichlorodihydrofluorescein diacetate (DCFH-DA) (0.1ug/mL) was added and incubated in darkness for 20 min. After 7 groups were all correspondingly treated, another 10-minute incubation was done. The production of ROS in each group was observed by Confocal laser scanning microscope (CLSM) (Nikon) (excitation/emission=502nm/530nm).

The Detection of DNA Double Strand Break

4T1 cells were seeded in confocal dishes at a concentration of 3*10^4 wells/dish and incubated overnight for attachment. Two hours after 7 groups were all correspondingly treated, the cells were fixed by 4% of paraformaldehyde for 10 min and washed by PBS, then incubated with 0.5% of Triton X-100 (dissolved in PBS) for 20-minute permeation at room

temperature. Cells were washed by PBS for three times, followed by one hour's block with 1% of BSA solution at room temperature and overnight incubation with the primary antibody (Anti-phospho-histone γ-H2AX Mouse monoclonal antibody, diluted by PBS, 1:500) at 4°C. Cells were washed by Phosphate buffered saline tween-20 (PBST) for three times and incubated with the secondary antibody (Goat Anti-Mouse IgG H&L) in darkness for 1 hour at room temperature. Then the cells were washed by PBS for 3 times and stained by 4',6-diamidino-2-phenylindole (DAPI). Finally, the cells were observed under CLSM (excitation/emission=495nm/519nm).

Cell Apoptosis Detected by Flow Cytometry

4T1 cells were seeded in 6-well plate at a concentration of $2*10^5$ cells/well and incubated overnight for attachment. After 7 groups were all correspondingly treated, the cells were digested, collected and centrifugated at 1000 rpm for 5 min to remove the cell culture medium. Then they were washed by PBS and centrifuged again to remove PBS, and pre-cooled ethanol (70%) was added to fix cells for 1–2 hours at 4 °C. The cells were centrifuged to remove ethanol, and resuspended by PBS for 5 min, followed by filtration by 400-mesh filter, and centrifuged at 1000 rpm for 5 min to remove PBS; then the cells were stained by 1 mL of PI for 30 min in darkness at 4°C. Finally, cell apoptosis of the prepared samples was analyzed by flow cytometry (excitation/emission=488nm/630nm) (Becton Dickinson). Q1-LL represents living cells, Q1-LR represents early apoptotic cells, Q1-UR represents late apoptotic cells, and Q1-UL represents nuclear debris.

CCK-8 assay: PIBD was applied at a dosage of 100 μL, 2.5mg/mL. ROS detection: PIBD was applied at a dosage of 1 mL, 2.5mg/mL. DNA double strand breakage detection: PIBD was applied at a dosage of 1 mL, 2.5mg/mL. Apoptosis detection by Flow Cytometry: PIBD was applied at a dosage of 2 mL, 2.5mg/mL.

In Vivo

Tumor-bearing mice were divided into the following groups: ①Control; ②PIBD; ③NIR; ④X-ray; ⑤X-ray+NIR; ⑥PIBD+NIR; ⑦PIBD+X-ray; ⑧PIBD+X-ray+NIR。X-ray was applied at a dosage of 6Gy; NIR was applied at a wavelength of 808nm, power was set at $1W/cm^2$. Other mice-related treatments were consistent with the imaging process.

Tumor-bearing mice were anesthetized by 1% of pentobarbitone, and intravenously injected with 200 μL of PIBD nanoparticles (5mg/mL). Corresponding treatments were conducted to all 8 groups. A near infrared thermal imager was used to record the fluctuation of temperature in group ①③⑥, and PA imager was used to detect the changes of blood oxygen in tumor areas before and after laser irradiation in group ③⑥. All 8 groups were treated accordingly, after which the tumor volumes and the weights of mice were measured and recorded every two days, and the whole treatment cycle lasted for 14 days. The tumor volume was calculated by the following equation: $V(cm^3) = (length*width)/2$. After treatment, mice were euthanized, and H&E staining was performed on tumor tissues and major organs including heart, liver, spleen, lung and kidney, PCNA, TUNEL and Immunofluorescence (IF) examinations were conducted to examine cell proliferation and apoptosis in tumors. The synergistic treatment effect was evaluated by Combination index (CI). Combination index (CI) is calculated by the following Equation: $CI = (D_{A|A+B})/D_A+(D_{B|A+B})/D_B$. Where $D_{A|A+B}$ and $D_{B|A+B}$ are the doses for RT and PTT in combined therapy, respectively, which are the half-maximal inhibitory concentration (IC50). D_A is the dose for RT and D_B is the dose for PTT, which are IC50 for 4T1 tumor. The CI value reflects the interaction effect of radiotherapy and photothermal therapy. $CI < 0.6$ suggests strong synergism; $0.6 < CI < 0.8$ indicates moderate synergism; $0.8 < CI < 0.9$ indicates slight synergism; and $0.9 < CI < 1.1$ indicates an additive effect.

Statistical Analysis

Measurement data was presented as Mean ± standard deviation. Data were analyzed by *t*-test when complied with the normal distribution, otherwise by Mann–Whitney *U*-test when not. $P < 0.05$ was considered as statistically significant difference. All the data were analyzed by SPSS 22.0 software.

Results and Discussion

PIBD nanoparticle was successfully synthesized by the double emulsification method (Figure 1A). Grossly, it appeared to be a tube of green emulsion (Figure 1B), with an average hydrated particle size of 250.7 ± 8.05 nm (Figure 1C) and an average

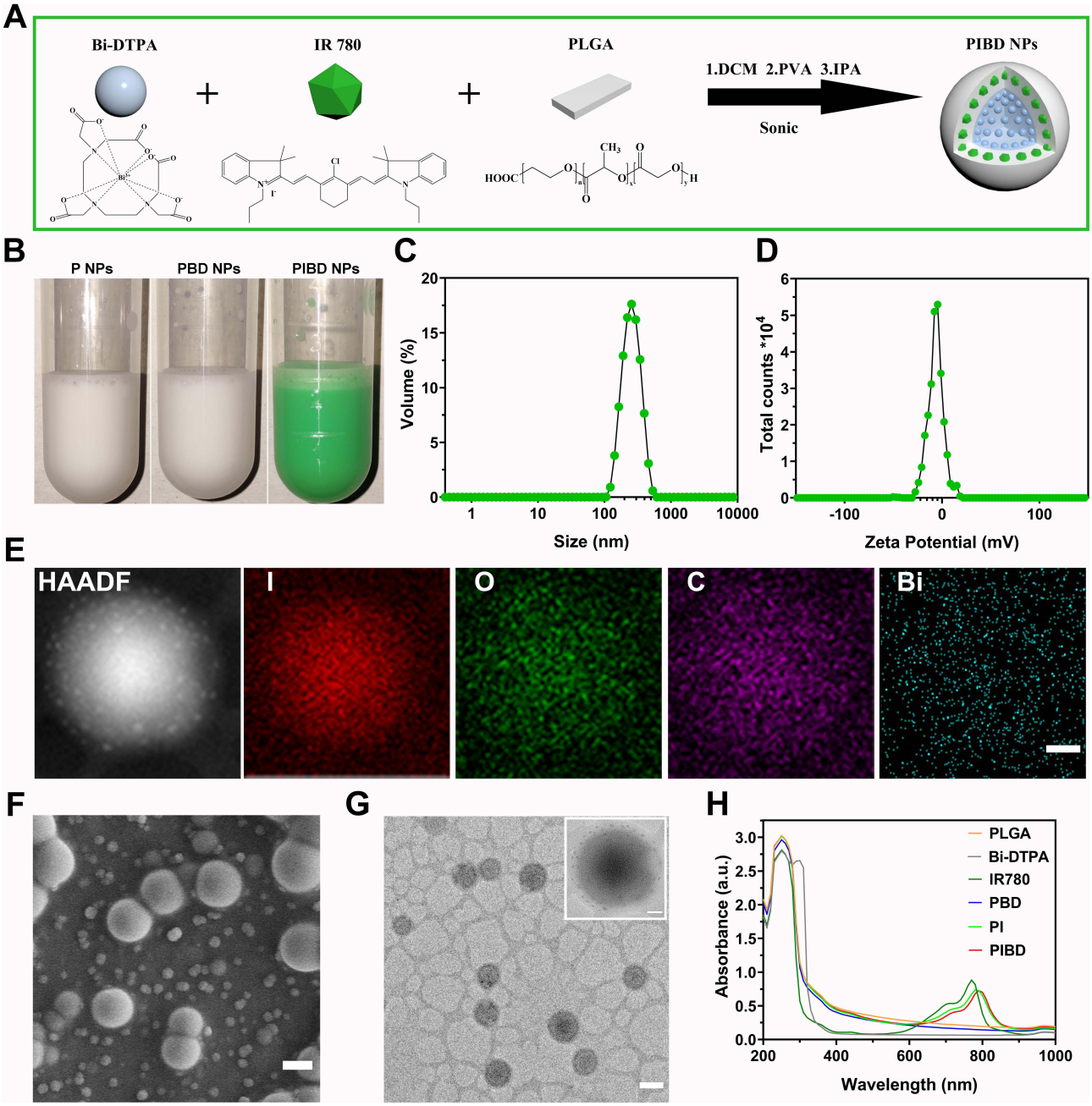

Figure 1 Characteristics of PIBD. (**A**) synthesized PIBD nanoparticle by double emulsification method; (**B**) observing PIBD with naked eyes; (**C**) zeta size of PIBD; (**D**) zeta potential of PIBD; (**E**) SEM-EDS images of PIBD (scale bar=50nm); (**F**) SEM captures of PIBD (scale bar=200nm); (**G**) TEM images of PIBD (scale bar=200nm or 50nm; (**H**) Wavelength detection by ultraviolet spectrophotometer of PIBD.

zeta potential at −4.81±1.94 mV (Figure 1D). After one week of observation and detection, the particle size of PIBD in serum did not change significantly, indicating that PIBD was very stable in serum (Figure S1). As shown in Figure 1E, the analyses on elements distribution demonstrated that C, O, I, Bi were uniformly distributed on nanoparticle areas. As observed by SEM, the nanoparticle presented a spherical morphology with the smooth surface and uniform size and good dispersibility (Figure 1F). Nanoparticles possessed a typical shell-core structure, as shown in the TEM image in Figure 1G. According to the results of UV spectrophotometer, the characteristic peak of Bi-DTPA at 260nm disappeared, while the characteristic peak of IR780 at 780nm was observed to have a decrease as well as the red shift, which indicated that the undetectable Bi-DTPA was loaded inside of PIBD, while the IR780 could still be detected since it was loaded on the surface of PIBD (Figure 1H). An

IR780 concentration/OD value standard curve was plotted (Figure S2), the encapsulation rate of IR780 was calculated to be 83.61 ± 1.61%, and the loading capacity was 3.34±0.06%. Bi-DTPA concentration/OD value standard curve was plotted (Figure S3) and the encapsulation rate of Bi-DTPA was calculated to be 98.32±0.6%, the loading capacity was 85.33 ± 1.08%. The upper limit value of the in vitro safety concentration was 2.5 mg/mL. When the cells were treated by nanoparticle at this concentration and below, the cell viability maintained over 90%, when the concentration was up-regulated to 3 mg/mL, the cell viability maintained over 80% (Figure S4). The results of blood routine examination and serum biochemistry examination showed that all the indexes were within the normal range, and there was no significant difference between mice in experimental groups (treated with nanoparticles) and mice in control group ($P > 0.05$). No abnormality was observed in H&E stained pathological sections of the main organs (Figures S5 and S6). Thus, the nanoparticle exhibited no obvious toxic and side effect in vitro and in vivo. After injection through the caudal vein, the content of Bi element in the blood gradually decreased, and approached 0 in 72h (Figure S7).

As shown in Figure 2, the fluorescence of DiI-tagged nanoparticles was represented as red, the cell nuclei stained by DAPI were blue, and the cell mitochondria marked by Mito-tracker green was green. After co-incubation, the overlapping areas of green fluorescence and red fluorescence in the PIBD group were significantly more than those in PBD group and control group. The Pearson's correlation coefficient (PCC) in PIBD group was 0.76 after Colocalization analysis, which was higher than 0.49 in control group and 0.48 in PBD group. The results indicated that PIBD efficiently targeted to mitochondria in 4T1 cells. Due to the higher negative transmembrane potential of tumor cell mitochondria, lipophilic cation IR780 preferentially accumulated in tumor cells rather than normal cells, endowing nanoparticles with good tumor-targeting ability.[26,29,30]

With the increase of nanoparticle concentration, the maximum temperature of photothermal effect was gradually promoted, maintaining at 50°C when the concentration of nanoparticles was 2.5mg/mL— the maximum biosafe concentration in vitro, and 60°C when 5 mg/mL—the maximum biosafe concentration in vivo. The time length to the

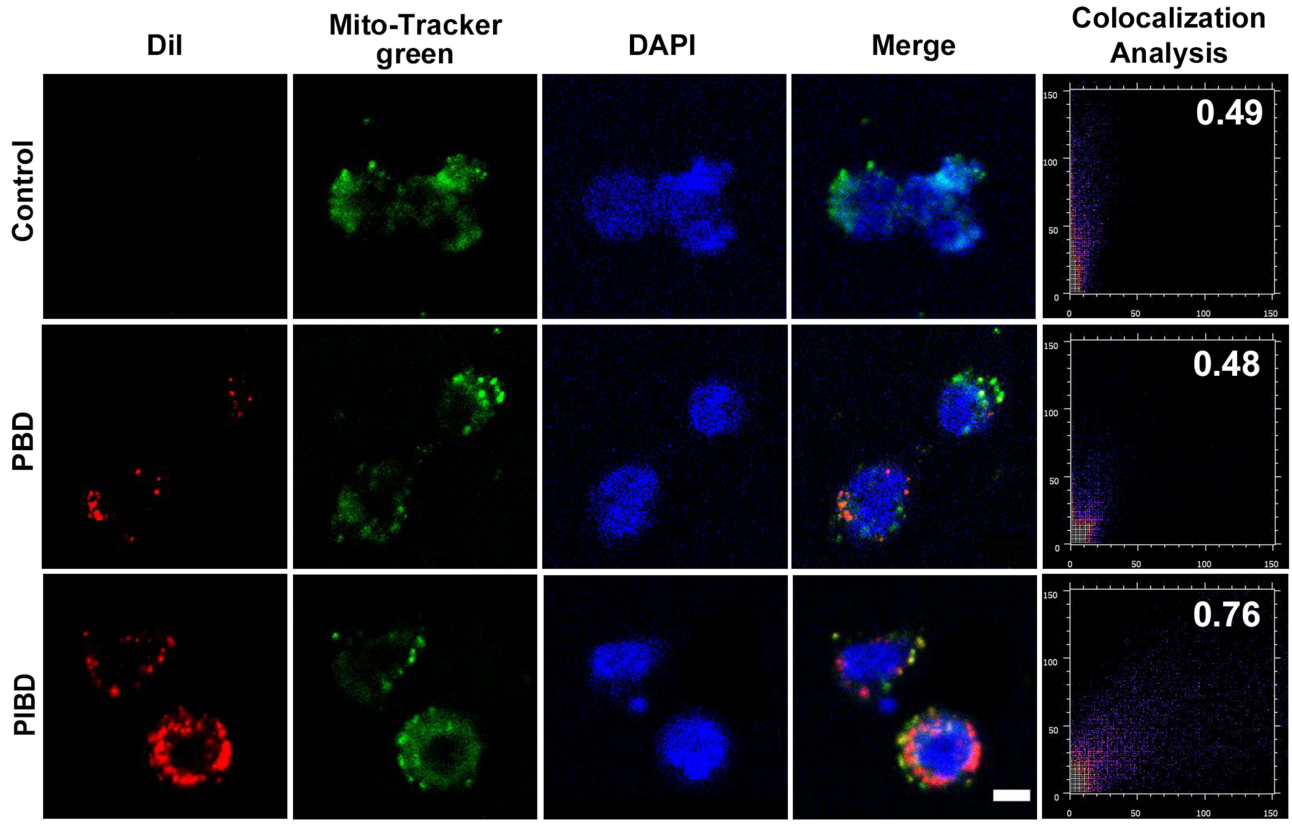

Figure 2 PIBD colocalized with mitochondrial as observed by CLSM (scale bar=10μm, colocalization quantitative analysis results were Pearson's correlation coefficient, −1 ~ 0.5 indicates no co-location. 0.5 ~ 1 indicates co-location).

maximum temperature was negatively correlated with the irradiation power. The temperature rapidly rose to 60°C within 1.5 minutes under the irradiation of 1W/cm^2 (Figure S8). According to in vitro photothermal effect detection, nanoparticles produced effective temperature over 47°C at a biosafe concentration,[31] exhibiting sound photothermal effect. Hence, 1W/cm^2 was selected as a standard therapeutic parameter during the following experiments.

With regard to the CT imaging characteristics of Bi-DTPA, PA and NIRF imaging characteristics of IR780, the multimode imaging capability of PIBD was further discussed. The strength of in vitro CT value/PA signals intensity and

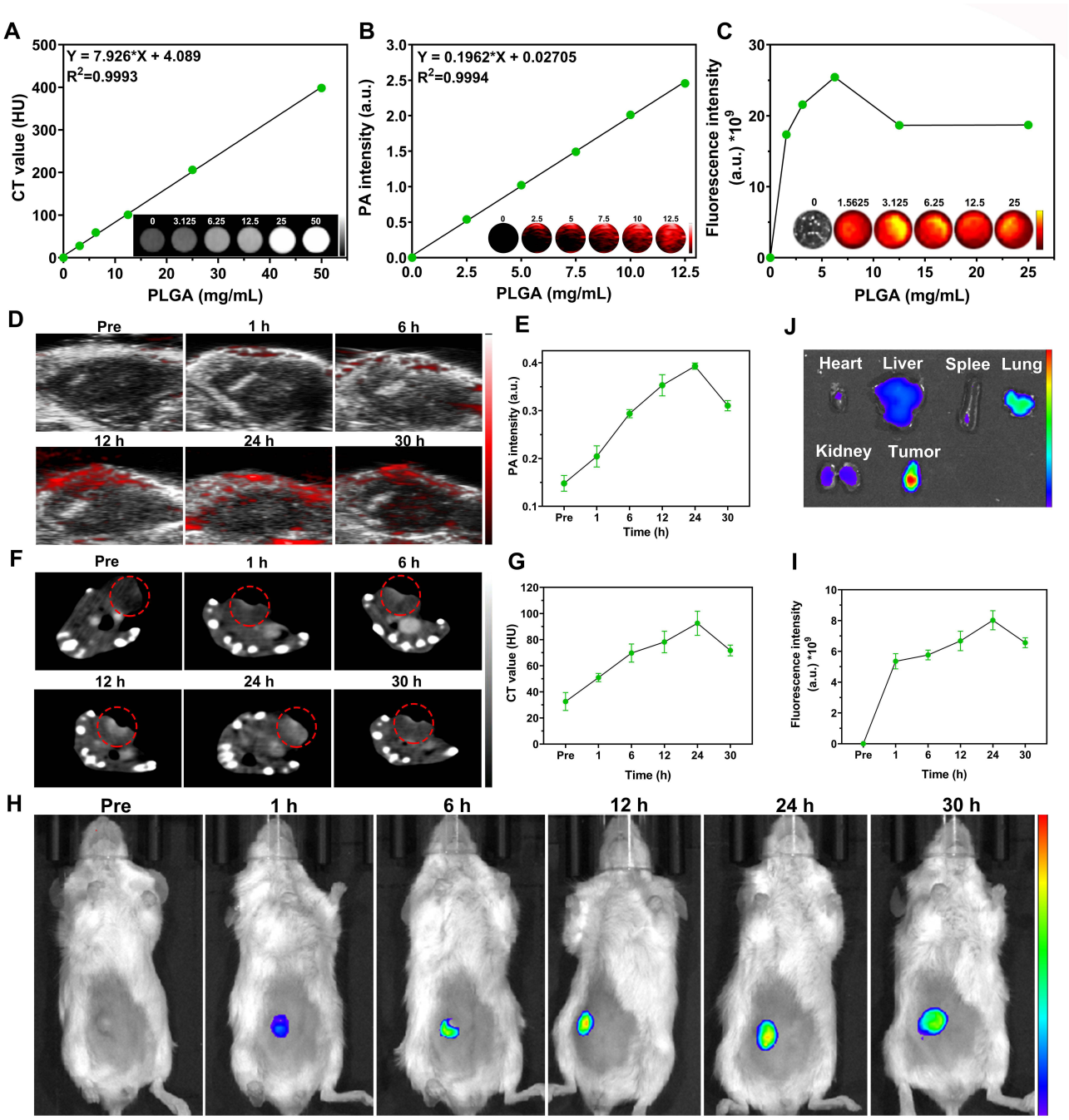

Figure 3 Multi-modality imaging by PIBD. (**A**) In vitro CT contrast images and CT values of PIBD at different concentrations; (**B**) In vitro PA contrast images and PA intensity of PIBD at different concentrations; (**C**) In vitro NIRF contrast images and NIRF intensity of PIBD at different concentrations; (**D**) In vivo PA images of tumors in 4T1 tumor-bearing mice after i.v. injection of PIBD at different time points; (**E**) Changes of PA-signal intensity within tumor regions at corresponding time points; (**F**) In vivo CT images of tumors in 4T1 tumor-bearing mice after i.v. injection of PIBD at different time points; (**G**) Changes of CT value within tumor regions at corresponding time points; (**H**) In vivo NIRF images of tumors in 4T1 tumor-bearing mice after i.v. injection of PIBD at different time points; (**I**) Changes of NIRF fluorescence intensity within tumor regions at corresponding time points; (**J**) In vivo NIRF images of tumor and organs in 4T1 tumor-bearing mice after i.v. injection of PIBD at 24h.

nanoparticle concentration followed a linear relation (Figure 3A and B). Similarly, the strength of the in vitro fluorescence intensity increased in a concentration-dependent manner, and reached its peak at a concentration of 6.25 mg/mL, after which the signal strength decreased when the concentration increased (Figure 3C). This phenomenon indicated that although IR780 endowed nanoparticles with NIRF imaging ability, cancellation occurred when concentration exceeded a certain boundary. The in vivo CT value/PA signal intensity in tumor sites increased in a time-dependent manner, where the peak value was detected at 24 hours (Figure 3D, E, F and G). The strength of the in vivo fluorescence intensity in the tumor area increased in a time-dependent manner, and reached its peak after 24 hours (Figure 3H and I). After 24 hours, fluorescence intensity in the tumor area was obviously stronger than that in the major organs ($P < 0.05$) (Figures 3J, S9), indicating the excellent tumor-targeting ability of the nanoparticle. No adverse reaction was observed in mice during all the imaging processes. As a newly-developed CT contrast agent, Bi-DTPA[24] has been proved to be feasible in breast cancer imaging in the previous part of the research. By loading Bi-DTPA in PLGA, CT imaging by nanoparticle was successfully achieved. By loading IR780 on PLGA, not only the hydrophobicity-caused application inconvenience of IR780 was addressed, but also the NIRF/PA imaging properties were achieved. Considering that the exceeded concentration of IR780 caused cancellation,[32] concentration at 5mg/mL was selected as an in vivo parameter for imaging and treatment, which ensured both biosafety and efficiencies in imaging and cancer treatment. Due to the tumor mitochondria-targeting ability of IR780,[26] fluorescent signal in tumor area was higher than that in major organs, which indicated the in vivo tumor-targeting ability of the nanoparticle and provided evidence and basis for the following targeted therapy.

In the following in vitro treatment, CCK8 assay results showed that, compared to cell viability in the control group (99.15 ± 5.67%), cell viability in group PIBD+X-ray+NIR, group PIBD+X-ray, group PIBD+NIR decreased to 3.24 ± 5.42%, 58.38 ± 3.28% and 41.77 ± 2.7%, respectively, and the differences were statistically significant ($P < 0.05$). Cell viability in X-ray, NIR, and X-ray+NIR slightly decreased to 87.3 ± 4.62%, 96.27 ± 13.2%, 86.46 ± 2.94% ($P < 0.05$) (Figure 4A), showing that cells were barely affected. Fluorescence intensity of ROS in PIBD+X-ray+NIR group was detected to be much stronger than that in group PIBD+X-ray, group PIBD+NIR or the sum of the two ($P < 0.05$), indicating that a 1+1>2 effect was achieved by the synergy between PTT and RT. Cells in group X-ray and group X-ray+NIR emitted weak fluorescence, while no obvious fluorescent was observed in cells in NIR group and the control group, as shown in Figure 4B and C. The DNA double strand breakage results showed that the fluorescence value of PIBD+X-ray+NIR group was detected to be apparently higher than that in PIBD+NIR and PIBD+X-ray or the sum of the two groups, indicating the combination of PTT and RT caused the largest numbers of damaged loci ($P<0.05$), while the weak fluorescence in X-ray group and X-ray+NIR group indicated that no obvious damaged locus was detected (Figure 4D and E). The highest apoptosis rate was detected in Group PIBD+X-ray+NIR (94.26±4.06%) ($P<0.05$), while the apoptosis rates in group PIBD +NIR, PIBD+X-ray, X-ray+NIR, NIR, X-ray and the control group were 35.33±2.09%, 33.33 ± 1.21%, 15.08±3.07%, 4.51 ± 0.91%, 13.68 ± 1.26% and 4.98 ± 1.89%, respectively (Figure 4F and G), which corresponded to the results mentioned above, indicating the synergy between PTT and RT in the combination therapy resulted in the best tumor-killing effect.

Referring to the results of in vivo treatment (Figure 5A), the temperature of the tumor area in PIBD+NIR group reached 50°C after 80 seconds, and stayed stable afterwards, while that in NIR group reached 40°C after 30 seconds, and remained 40°C afterwards; in control group, the temperature maintained at 33°C with no obvious fluctuation through the whole experiment process (Figure 5B and C). The blood oxygen content in PIBD+NIR group increased from 29.63 ± 3.17% (pre-treatment) to 58 ± 4.43% after NIR irradiation ($P < 0.05$), while that in the NIR group had no significant change ($P > 0.05$) (Figure 5D and E). As demonstrated by the change of tumor volume, tumors volume in PIBD+X-ray +NIR shrank to an immeasurable level and was recorded as 0, while tumor volumes in PIBD+X-ray group and PIBD +NIR group shrank to some extent, but still measurable, and the difference in tumor volume change between the two groups was not statistically significant ($P > 0.05$); the elimination of tumors in X-ray+NIR group and X-ray group was much less obvious than that in groups described above, and the difference in tumor volume change between the two groups was not statistically significant ($P > 0.05$). Tumors in NIR group, PIBD group and control group presented rapid growth rather than elimination, and no significant difference was found among the three groups ($P > 0.05$) (Figure 5F and G). The result of CI was 0.662, indicating that PTT-RT-combined therapy had a moderate synergism inhibitory effect on tumor. The results of H&E staining showed that the nuclei in the sections of tumor tissues in PIBD+X-ray+NIR group were barely distinguishable, indicating that severe damages occurred. Nucleolysis was observed in PIBD+X-ray and

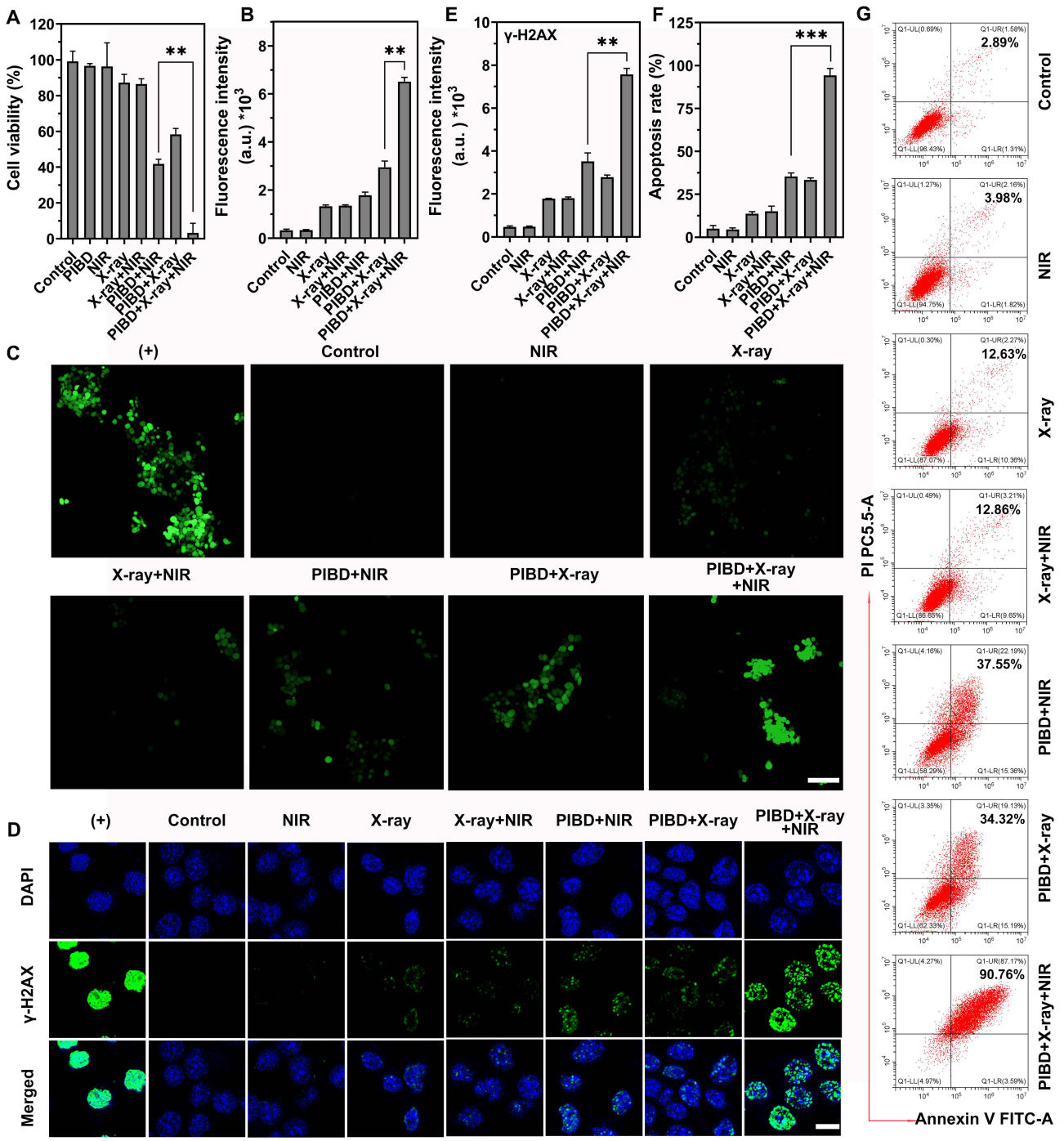

Figure 4 In vitro treatment. (**A**) Cell viability of 4T1 cells in different treatments by CCK8 assay; (**B**) Fluorescence intensity of DCFH-DA by different treatments; (**C**) Enhanced ROS production by PIBD in 4T1 cells. Confocal images (green fluorescence indicates positive staining for ROS stained with DCFH-DA) by different treatments (scale bar=100 μm); (**D**) DNA double strand breakage by PIBD in 4T1 cells. Confocal images (green fluorescence indicates positive staining for DNA double strand breakage stained with γ-H2AX) by different treatments (scale bar=10 μm). (**E**) Fluorescence intensity of γ-H2AX by different treatments; (**F**) Apoptosis rate of 4T1 cells in different treatments; (**G**) Apoptosis of 4T1 cells in different treatments by flow cytometry. (**P<0.01, ***P<0.001).

PIBD+NIR group, and only a small part of tumor cells in X-ray+NIR and X-ray group were damaged, while no obvious damage was observed in the NIR group, PIBD group and the control group. No significant damage was found in the normal tissue of the tumor margin (Figure S10). The PCNA detection of tumor tissues showed that proliferating tumor cells were barely observed in PIBD+X-ray+NIR group, while cell proliferation in PIBD+X-ray and PIBD+NIR group was obviously inhibited, while inhibited cell proliferation was observed in only small part of cells in X-ray+NIR and

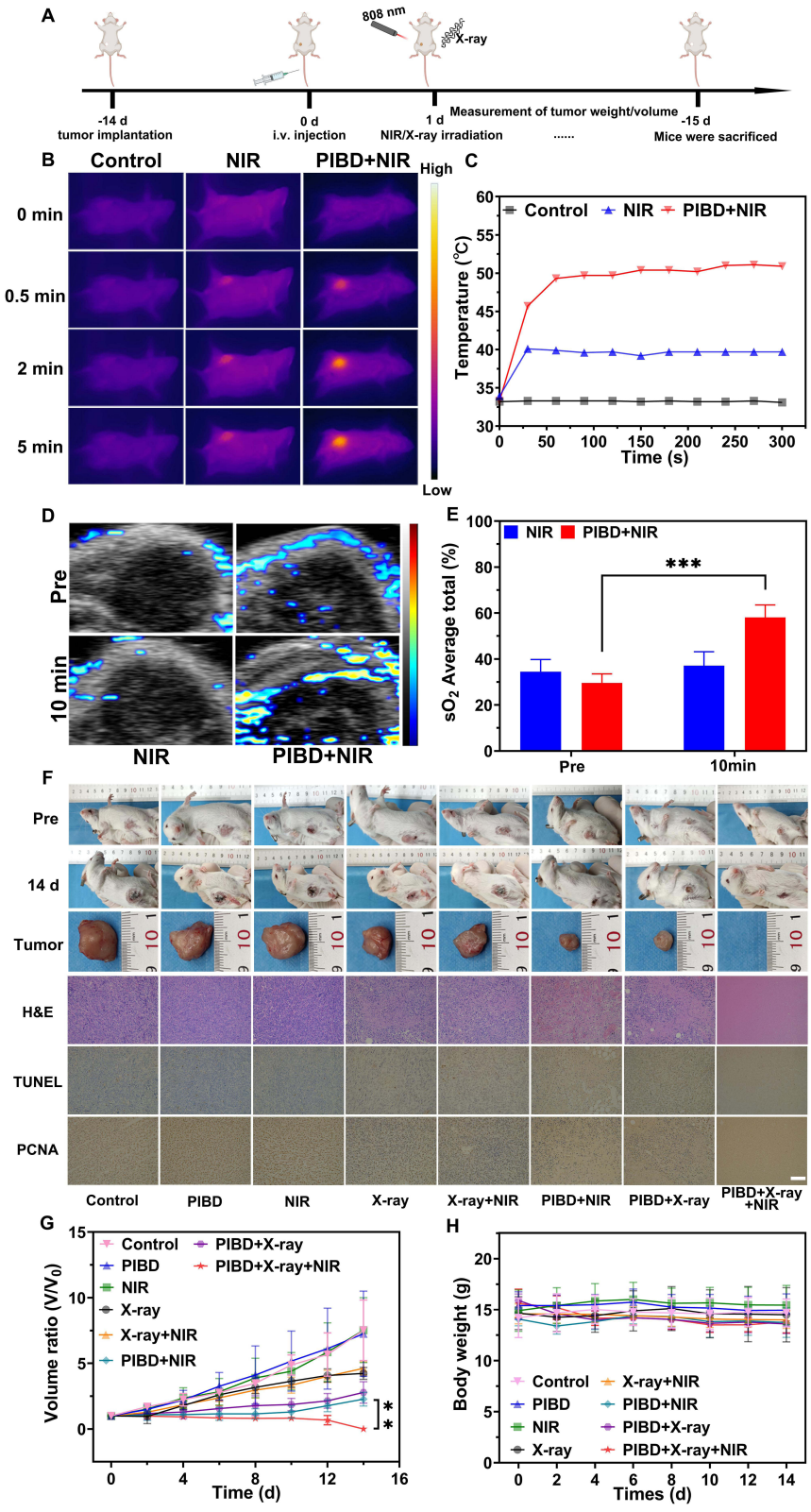

Figure 5 In vivo treatment by PIBD. (**A**) In vivo therapeutic process; (**B**) Thermal imaging of tumors in different treatments; (**C**) The corresponding time–temperature curves in different treatments; (**D**) PA blood oxygen imaging fore/post laser irradiation in different treatments; (**E**) The comparison of blood oxygen content in different treatments; (**F**) Tumor growth situations of tumor-bearing mice in different treatments, the corresponding results of H&E staining, PCNA and TUNEL detection (scale bar= 50 μm); (**G**) The curve of tumor size in different treatments through the whole treating process; (**H**) Weight change curve of tumor-bearing mice in different treatments. (compared with Control group **P<0.01, ***P<0.001).

X-ray group, and the proliferation in NIR, PIBD and the control group was not affected. The TUNEL detection of tumor tissue showed that apoptosis occurred in almost all tumor cells in PIBD+X-ray+NIR group, a large part of cells in PIBD +X-ray and PIBD+NIR group, and a small part of cells in X-ray+NIR and X-ray group, while cells in NIR, PIBD and the control group was not affected (Figure 5F). The results of IF staining were also the same as TUNEL, but the results of HIF-1α staining showed that the PIBD+NIR group had a decrease compared with the NIR group, while the PIBD+X-ray group had an increase compared with the X-ray group (Figure S10). H&E sections of major organs in all groups showed no obvious injury (Figure S11). The weight of mice in all groups had no obvious loss, and the difference between groups was not statistically significant ($P > 0.05$) (Figure 5H).

According to in vitro/vivo therapeutic results, comparing to either PTT only or RT only, the viability of 4T1 cells received both PTT and RT treatments significantly decreased, with more grievous DNA damage and apoptosis, when nanoparticles were applied at the maximum biosafe concentration, proving that the combined therapy compensated for the shortcomings of single therapy and showed better effectiveness. In details, IR780-induced photothermal effect accelerated the blood circulation in tumor area, consequently promoted oxygen content and reduced the level of hypoxic factor HIF-1α to relieved TME hypoxia,[16,17] by which the production of ROS was facilitated and RT efficiency was enhanced. Under the verified biosafe concentration, tumor growth was effectively inhibited, without any obvious adverse effect on normal tissues, proving that nanoparticles functioned as a combiner and a sensitizer to enhance radiotherapy.

With systematical analyses of current data, we have concluded several mechanisms of this PTT-RT-combined therapy. The photothermal effect induced by PIBD was verified in vitro and vivo. The in vivo photothermal effect caused an increase of temperature to 50°C within tumor areas. Hyperthermia (>47°C)[31] can directly kill tumor cells. The ROS can react with macromolecules such as DNA and proteins due to the strong oxidizing property, which induces tumor cell injuries.[33,34] PTT and RT both produced more ROS when assisted by nanoparticles. Furthermore, over-abundant ROS produced by the combined therapy and the consequent DNA damage all together surpassed the summation of two single treatments, and compensated for each other's shortcomings in treatment. Thermal effect can accelerate blood circulation in tumor areas, resulting in the reverse of tumor microenvironment hypoxia,[16,17] with the application of nanoparticles plus laser radiation, the blood oxygen content in tumor areas was promoted significantly and reduced the level of hypoxic factor HIF-1α. The reverse of hypoxia facilitated the production of oxygen-dependent ROS of RT,[27] compensating for the incompleteness of the single PTT treatment. The mechanism above may explain for the synergistic effect of the combined therapy. No abnormality was observed in H&E staining of pathological sections of the main organs, indicating the good biosafety and targeted biodistribution of the nanoparticle. PIBD realized the enhancement of tumor killing effect by lower dosage of RT and avoided unwanted adverse effects on normal tissues, which provided a safer and more efficient way to treat cancer.

Conclusion

In this study, PIBD nanoparticle was properly designed and successfully synthesized to enhance RT sensitivity and reduce RT side effects. It possesses good tumor-targeting ability and biosafety. Moreover, the thermal effect produced by the nanoparticle under laser radiation not only injured tumor tissues, but also reversed TEM hypoxia and consequently enhanced the production of oxygen-dependent ROS during RT, which compensated for the shortcoming of PTT in treating deep lesions. Except for overcoming the limitation of single therapy either by PTT or RT, nanoparticle also presented good behaviors in multi-modality imaging, including PA, NIRF imaging and CT, providing an efficient and safe theranostic method.

Ethics Approval and Consent to Participate

The animal experiments in this study have been approved by the Ethics Committee of the First Affiliated Hospital of Chongqing Medical University (IACUC-CQMU-2023-0252)

Comply with "the Regulations on the Management of Laboratory Animals", "the Guiding Opinions on the Treatment of Laboratory Animals", "the Guidelines on the Ethical Review of the Welfare of Laboratory Animals" and Chongqing Medical University experimental animal regulations.

Acknowledgments

Authors are thankful to the National Natural Science Foundation of China support of this study. We are also grateful to the Oncology Department of the First Affiliated Hospital of Chongqing Medical University for their technical supports.

Author Contributions

All authors contributed to data analysis, drafting or revising the article, have agreed on the International Journal of Nanomedicine to which the article will be submitted, gave final approval of the version to be published, and agree to be accountable for all aspects of the work.

Funding

This work was funded by the National Natural Science Foundation of China (Grant Numbers 82071926, 81630047), Chongqing Natural Science Foundation project (CSTB2022NSCQ-MSX1384).

Disclosure

The authors report no conflicts of interest in this work.

References

1. Braunstein LZ, Bellon JR. Contemporary issues in breast cancer radiotherapy. *Hematol Oncol Clin North Am*. 2020;34(1):1–12. doi:10.1016/j.hoc.2019.08.014
2. Dong J, Li Y, Xiao H, et al. Cordycepin sensitizes breast cancer cells toward irradiation through elevating ROS production involving Nrf2. *Toxicol Appl Pharmacol*. 2019;364:12–21. doi:10.1016/j.taap.2018.12.006
3. Azzam EI, Jay-Gerin JP, Pain D. Ionizing radiation-induced metabolic oxidative stress and prolonged cell injury. *Cancer Lett*. 2012;327(1–2):48–60. doi:10.1016/j.canlet.2011.12.012
4. Jarosz-Biej M, Smolarczyk R, Cichoń T, Kułach N. Tumor microenvironment as a "game changer" in cancer radiotherapy. *Int J Mol Sci*. 2019;20(13):1.
5. Xie J, Gong L, Zhu S, Yong Y, Gu Z, Zhao Y. Emerging strategies of nanomaterial-mediated tumor radiosensitization. *Adv Mater*. 2019;31(3):e1802244. doi:10.1002/adma.201802244
6. Peitzsch C, Kurth I, Ebert N, Dubrovska A, Baumann M. Cancer stem cells in radiation response: current views and future perspectives in radiation oncology. *Int J Radiat Biol*. 2019;95(7):900–911. doi:10.1080/09553002.2019.1589023
7. Guo Z, Zhu S, Yong Y, et al. Synthesis of BSA-Coated BiOI@Bi(2) S(3) semiconductor heterojunction nanoparticles and their applications for radio/photodynamic/photothermal synergistic therapy of tumor. *Adv Mater*. 2017;29(44):1.
8. Cheng X, Yong Y, Dai Y, et al. Enhanced radiotherapy using bismuth sulfide nanoagents combined with photo-thermal treatment. *Theranostics*. 2017;7(17):4087–4098. doi:10.7150/thno.20548
9. Zhang F, Liu H, Duan M, et al. Crosstalk among m(6)A RNA methylation, hypoxia and metabolic reprogramming in TME: from immunosuppressive microenvironment to clinical application. *J Hematol Oncol*. 2022;15(1):84. doi:10.1186/s13045-022-01304-5
10. Barker HE, Paget JT, Khan AA, Harrington KJ. The tumour microenvironment after radiotherapy: mechanisms of resistance and recurrence. *Nat Rev Cancer*. 2015;15(7):409–425. doi:10.1038/nrc3958
11. Yin H, Sun L, Pu Y, et al. Ultrasound-Controlled CRISPR/Cas9 system augments sonodynamic therapy of hepatocellular carcinoma. *ACS Cent Sci*. 2021;7(12):2049–2062. doi:10.1021/acscentsci.1c01143
12. Zhou X, You M, Wang F, et al. Multifunctional graphdiyne-cerium oxide nanozymes facilitate MicroRNA delivery and attenuate tumor hypoxia for highly efficient radiotherapy of esophageal cancer. *Adv Mater*. 2021;33(24):e2100556. doi:10.1002/adma.202100556
13. Liang B, Qiao B, Yu K, et al. Mitochondrial glutathione depletion nanoshuttles for oxygen-irrelevant free radicals generation: a cascaded hierarchical targeting and theranostic strategy against hypoxic tumor. *ACS Appl Mater Interfaces*. 2022;14(11):13038–13055. doi:10.1021/acsami.1c24708
14. Cui L, Gouw AM, LaGory EL, et al. Mitochondrial copper depletion suppresses triple-negative breast cancer in mice. *Nat Biotechnol*. 2021;39(3):357–367. doi:10.1038/s41587-020-0707-9
15. Murphy MP, Hartley RC. Mitochondria as a therapeutic target for common pathologies. *Nat Rev Drug Discov*. 2018;17(12):865–886. doi:10.1038/nrd.2018.174
16. Lv W, Cao M, Liu J, Hei Y, Bai J. Tumor microenvironment-responsive nanozymes achieve photothermal-enhanced multiple catalysis against tumor hypoxia. *Acta Biomater*. 2021;135:617–627. doi:10.1016/j.actbio.2021.08.015
17. Zhang B, Xu C, Sun C, Yu C. Polyphosphoester-based nanocarrier for combined radio-photothermal therapy of breast cancer. *ACS Biomater Sci Eng*. 2019;5(4):1868–1877. doi:10.1021/acsbiomaterials.9b00051
18. Beik J, Abed Z, Ghoreishi FS, et al. Nanotechnology in hyperthermia cancer therapy: from fundamental principles to advanced applications. *J Control Release*. 2016;235:205–221. doi:10.1016/j.jconrel.2016.05.062
19. Amini SM. Gold nanostructures absorption capacities of various energy forms for thermal therapy applications. *J Therm Biol*. 2019;79:81–84. doi:10.1016/j.jtherbio.2018.12.007
20. Yeh BM, FitzGerald PF, Edic PM, et al. Opportunities for new CT contrast agents to maximize the diagnostic potential of emerging spectral CT technologies. *Adv Drug Deliv Rev*. 2017;113:201–222. doi:10.1016/j.addr.2016.09.001
21. Griffith DM, Li H, Werrett MV, Andrews PC, Sun H. Medicinal chemistry and biomedical applications of bismuth-based compounds and nanoparticles. *Chem Soc Rev*. 2021;50(21):12037–12069. doi:10.1039/d0cs00031k

22. Wu B, Lu ST, Yu H, et al. Gadolinium-chelate functionalized bismuth nanotheranostic agent for in vivo MRI/CT/PAI imaging-guided photothermal cancer therapy. *Biomaterials*. 2018;159:37–47. doi:10.1016/j.biomaterials.2017.12.022
23. Li L, Lu Y, Jiang C, et al. Actively targeted deep tissue imaging and photothermal-chemo therapy of breast cancer by antibody-functionalized drug-loaded X-Ray-responsive bismuth sulfide@mesoporous silica core-shell nanoparticles. *Adv Funct Mater*. 2018;28(5):3.
24. Liao W, Lei P, Pan J, et al. Bi-DTPA as a high-performance CT contrast agent for in vivo imaging. *Biomaterials*. 2019;203:1–11. doi:10.1016/j.biomaterials.2019.03.001
25. Zhang Y, Liu D, Qiao B, et al. Bi-DTPA, a potential CT-guided radiation sensitizer. *Biochem Biophys Res Commun*. 2023;671:192–199. doi:10.1016/j.bbrc.2023.05.065
26. Zhang C, Liu T, Su Y, et al. A near-infrared fluorescent heptamethine indocyanine dye with preferential tumor accumulation for in vivo imaging. *Biomaterials*. 2010;31(25):6612–6617. doi:10.1016/j.biomaterials.2010.05.007
27. Oei AL, Kok HP, Oei SB, et al. Molecular and biological rationale of hyperthermia as radio- and chemosensitizer. *Adv Drug Deliv Rev*. 2020;163–164:84–97. doi:10.1016/j.addr.2020.01.003
28. Shi S, Liu Y, Chen Y, et al. Versatile pH-response micelles with high cell-penetrating helical diblock copolymers for photoacoustic imaging guided synergistic chemo-photothermal therapy. *Theranostics*. 2016;6(12):2170–2182. doi:10.7150/thno.16633
29. Davis S, Weiss MJ, Wong JR, Lampidis TJ, Chen LB. Mitochondrial and plasma membrane potentials cause unusual accumulation and retention of rhodamine 123 by human breast adenocarcinoma-derived MCF-7 cells. *J Biol Chem*. 1985;260(25):13844–13850.
30. Modica-Napolitano JS, Aprille JR. Basis for the selective cytotoxicity of rhodamine 123. *Cancer Res*. 1987;47(16):4361–4365.
31. Ghaffari H, Beik J, Talebi A, Mahdavi SR, Abdollahi H. New physical approaches to treat cancer stem cells: a review. *Clin Transl Oncol*. 2018;20(12):1502–1521. doi:10.1007/s12094-018-1896-2
32. Zhu M, Sheng Z, Jia Y, et al. Indocyanine green-holo-transferrin nanoassemblies for tumor-targeted dual-modal imaging and photothermal therapy of glioma. *ACS Appl Mater Interfaces*. 2017;9(45):39249–39258. doi:10.1021/acsami.7b14076
33. Srinivas US, Tan BWQ, Vellayappan BA, Jeyasekharan AD. ROS and the DNA damage response in cancer. *Redox Biol*. 2019;25:101084. doi:10.1016/j.redox.2018.101084
34. Wen J, Luo Y, Gao H, et al. Mitochondria-targeted nanoplatforms for enhanced photodynamic therapy against hypoxia tumor. *J Nanobiotechnology*. 2021;19(1):440. doi:10.1186/s12951-021-01196-6